

Dissolved organic matter photolysis in Canadian arctic thaw ponds

This content has been downloaded from IOPscience. Please scroll down to see the full text.

2013 Environ. Res. Lett. 8 035026

(<http://iopscience.iop.org/1748-9326/8/3/035026>)

View [the table of contents for this issue](#), or go to the [journal homepage](#) for more

Download details:

IP Address: 198.73.161.137

This content was downloaded on 22/11/2013 at 14:54

Please note that [terms and conditions apply](#).

Dissolved organic matter photolysis in Canadian arctic thaw ponds

Isabelle Laurion^{1,2} and Natalie Mladenov³

¹ Centre d'études nordiques, U Laval, Québec, QC, Canada

² Institut National de la Recherche Scientifique, Centre Eau Terre Environnement, Québec, QC, G1K 9A9, Canada

³ Department of Civil Engineering, Kansas State University, Manhattan, KS 66506, USA

E-mail: Isabelle.laurion@ete.inrs.ca

Received 28 February 2013

Accepted for publication 15 July 2013

Published 5 August 2013

Online at stacks.iop.org/ERL/8/035026

Abstract

The abundant thaw lakes and ponds in the circumarctic receive a new pool of organic carbon as permafrost peat soils degrade, which can be exposed to significant irradiance that potentially increases as climate warms and ice cover shortens. Exposure to sunlight is known to accelerate the transformation of dissolved organic matter (DOM) into molecules that can be more readily used by microbes. We sampled the water from two common classes of ponds found in the ice-wedge system of continuous permafrost regions of Canada, polygonal and runnel ponds, and followed the transformation of DOM over 12 days by looking at dissolved organic carbon (DOC) concentration and DOM absorption and fluorescence properties. The results indicate a relatively fast decay of color (3.4 and 1.6% loss d⁻¹ of absorption at 320 nm for the polygonal and runnel pond, respectively) and fluorescence (6.1 and 8.3% loss d⁻¹ of total fluorescent components, respectively) at the pond surface, faster in the case of humic-like components, but insignificant losses of DOC over the observed period. This result indicates that direct DOM mineralization (photochemical production of CO₂) is apparently minor in thaw ponds compared to the photochemical transformation of DOM into less chromophoric and likely more labile molecules with a greater potential for microbial mineralization. Therefore, DOM photolysis in arctic thaw ponds can be considered as a catalytic mechanism, accelerating the microbial turnover of mobilized organic matter from thawing permafrost and the production of greenhouse gases, especially in the most shallow ponds. Under a warming climate, this mechanism will intensify as summers lengthen.

Keywords: DOM, photobleaching, thermokarst lakes, permafrost

1. Introduction

Lakes and ponds are ubiquitous features of permafrost landscapes (Rautio *et al* 2011). Smith *et al* (2007) estimated that more than 140 000 lakes with an area from 0.1 to 50 km² now cover a total area of almost 400 000 km² in the circumarctic permafrost landscape. This area, estimated

from the global lakes and wetlands database of Lehner and Döll (2004), is conservative considering that most tundra ponds are much smaller than 0.1 km², corresponding to a water body with a diameter of 357 m. An abundant class of tundra ponds, thaw ponds, are generated when ice-rich ground subsides naturally in summer or as a response to accelerated warming, a process characterized by thermokarst erosion in organic ground (Fortier and Allard 2004, Rowland *et al* 2010). Longer summers, warmer air temperatures and increased precipitation in polar regions degrade permafrost and increase carbon (C) inputs to aquatic ecosystems (Grosse *et al* 2011,



Content from this work may be used under the terms of the [Creative Commons Attribution 3.0 licence](http://creativecommons.org/licenses/by/3.0/). Any further distribution of this work must maintain attribution to the author(s) and the title of the work, journal citation and DOI.

IPCC 2007), both from an old C pool from eroding peat in thermokarst slumps (Kuhry *et al* 2009) and from a more recent pool associated with growing plants, plankton and benthic microbial mats. Additional climate change-driven carbon mobilization from permafrost soils raises concern because of its potential to act as a positive feedback mechanism on climate through microbial production of greenhouse gases (GHG; Walter *et al* 2007, Laurion *et al* 2010, Abnizova *et al* 2012). Climate change also influences thermal stratification strength and irradiance regime in lakes through its effect on ice cover duration and concentration of optically active substances (Zepp *et al* 2007, Prowse *et al* 2011, Vincent *et al* 2013). These changes likely affect photochemical and microbial breakdown of the mobilized C, part of which is liberated to the atmosphere as GHG.

Photolysis of dissolved organic matter (DOM) represents a significant C mineralization process, which depends on its composition or photoreactivity and on its exposure to ultraviolet (UV) radiation (Vähätalo *et al* 2000, Johannessen and Miller 2001). For example, Bélanger *et al* (2006) estimated that almost 3% of annual dissolved organic C (DOC) delivered to the southeastern Beaufort Sea via the Mackenzie River was photomineralized into dissolved inorganic C (DIC), representing ~10% of the bacterial respiration. Moreover, the study shows how the reduction in the duration of sea ice cover will likely increase the importance of this mineralization process. Direct photomineralization of DOM also represented approximately 10% of dark respiration in the epilimnion of boreal lakes (Granéli *et al* 1996). Most photochemical mineralization in the water column took place in the top 10 cm of a humic lake in Finland (Vähätalo *et al* 2000).

The absorption of light by chromophoric DOM molecules (CDOM) also causes structural changes in organic molecules, decreasing their capacity to further absorb light, a process known as photobleaching or photolysis, and reducing the molecular weight (Bertilsson and Allard 1996). Photochemical degradation of DOM is considered a major sink of DOM in surface layers of lakes, with large variations in photolysis rates between lakes primarily depending on light exposure, but also on pH or acid-neutralizing capacity (Reche *et al* 1999, Bertilsson and Tranvik 2000). CDOM loss can significantly increase the exposure of aquatic communities to UV. For example, CDOM loss was observed as large declines in UV attenuation over the open water season in arctic ponds of the Mackenzie Delta (Gareis *et al* 2010). This is particularly relevant for shallow ponds commonly found in the arctic tundra. Perhaps more importantly, DOM photolysis can stimulate microbial activity through its action on DOM lability (Lindell *et al* 1995), and therefore accelerate DOM mineralization and C cycling. Irradiated humic substances were shown to enhance bacterial C production, respiration and growth efficiency (Anesio *et al* 2005). Obernosterer and Benner (2004) have demonstrated that biological and photochemical processes can compete in the mineralization of DOC.

In an experiment exposing lake DOM to natural sunlight for 70 days, solar radiation decomposed 96% of freshwater

CDOM but only 41% of DOC, and UV radiation was responsible for 75% of this decomposition at the surface of the water column (Vähätalo and Wetzel 2004). This study also shows that the natural plankton community needed 500 days to decompose in the dark as much CDOM as was decomposed by solar radiation at the surface in a week. Photolysis can be measured as losses of bulk DOC, which include both CDOM and non-chromophoric DOM, or changes in CDOM properties such as fluorescence and absorption at specific wavelengths. A simple index developed by Loiselle *et al* (2009), the spectral slope signature S_{λ} , provides additional insights into DOM losses. Another informative tool is provided by the extraction of CDOM fluorescent components using excitation–emission matrices (EEMs) and parallel factor analysis (PARAFAC; Stedmon *et al* 2003), where the dynamics of individual chromophores or groups of chromophores can be studied (Chen *et al* 2003).

DOM photolysis in arctic thaw ponds located on organic landscapes may be particularly important for C cycling in summer, especially for the shallowest ponds and since they are exposed to 24 h of daylight and constantly supplied by fresh organic matter inputs as the active layer thaws. The peat soils surrounding ponds, accumulated during the Holocene in northeastern Canada, are now mobilized as permafrost degrades and erosion occurs (figure 1). Several ponds are also colonized by thick microbial mats (Vézina and Vincent 1997) and macrophytes (Tank *et al* 2009), which actively produce organic compounds taking part in the C cycle (Bertilsson and Jones 2003). In previous studies done on Bylot Island, thaw ponds were shown to be particularly rich in nutrients and DOM, dominated by active microbial food webs, and to emit substantial amounts of methane, and sometimes CO₂, to the atmosphere (Breton *et al* 2009, Laurion *et al* 2010). DOM was found to have variable contributions from allochthonous and autochthonous sources. The nature of DOM in arctic thaw ponds and the rate at which it is being transformed needs to be determined in order to estimate its importance to microbial activity, GHG production and C burial (Tranvik *et al* 2009). As climate shifts in the Arctic, several factors influencing DOM, light exposure and microbial activity are changing; therefore simple GHG flux measurements are not sufficient to adequately predict future climate change and feedback in such dynamic systems. The objective of the study was to quantify photolysis rates and examine photochemical transformation of DOM in two contrasting arctic thaw ponds commonly found in the continuous permafrost landscape, by tracking changes in DOM optical properties and DOC concentrations over 12 days using *in situ* incubations.

2. Methods

Thaw ponds were investigated in Sirmilik National Park on Bylot Island, Nunavut, in northern Canada, in the continuous permafrost tundra (73°09'N, 79°58'W; figure 1). The ice-wedge tundra terrain sampled lies along a pro-glacial river valley covered by a network of ponds, similar to the landscape of Samoylov Island in Eastern Siberia (Muster *et al*

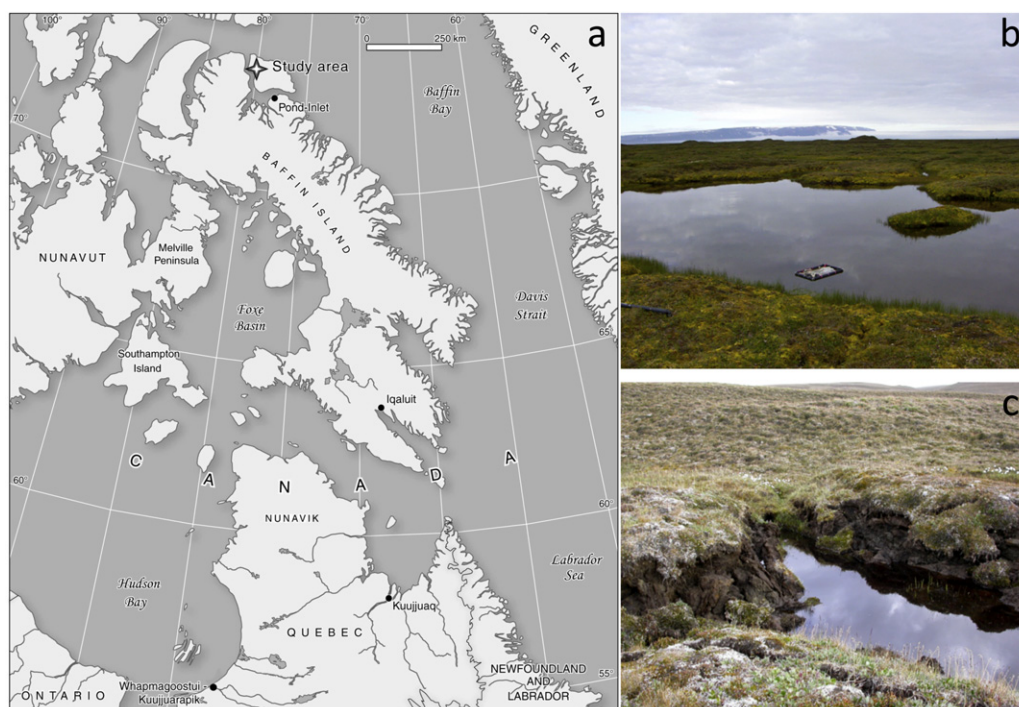


Figure 1. Site location (a) and photos of ponds BYL1 (b) and BYL38 (c).

2012), and covering 4.2% of the ~ 65 km² glacial valley. The base of the peat deposit, which is about 2 m thick, was aged at 3670 ± 110 BP (Fortier and Allard 2004), and the active layer reaches between 40 and 60 cm (Fortier 2013). The meteorological station of the field camp (SILA network station of the Centre for Northern studies) recorded a mean annual air temperature of -14.5°C , and about 94 mm of precipitation between June and August from 1994 to 2007. The vegetation surrounding the ponds is characterized by the presence of sedges, grasses and brown mosses species.

In this region, abundant ponds are formed at the surface of the permafrost terrain and separate in two major classes: 1—ponds on top of low-center peat polygons (Abnizova *et al* 2012), colonized by thick microbial mats (called *polygonal ponds* hereafter), and 2—water channels surrounding peat polygons formed over melting ice wedges, characterized by thermokarst slumping, peat erosion and high humic content (called *runnel ponds* hereafter as in Laurion *et al* (2010)). One pond of each type was chosen to perform *in situ* photolysis incubations. Teflon bottles (60 ml; UV transparent) filled with $0.2 \mu\text{m}$ -filtered water (using pre-rinsed cellulose acetate filters of $0.2 \mu\text{m}$ pore size; advantec micro filtration systems) were incubated at the pond surface at ~ 5 cm depth over 12 days between 18 and 31 July 2009. Replicate bottles were taken at 1, 2, 4, 6, 8 and 12 days (2, 6, and 12 days for dark control bottles) and stored in the dark and cold until analyses were performed (within two weeks after the end of experiment). Bulk concentrations of DOC, and absorption and fluorescence properties of CDOM were measured. The efficiency of filtration to remove bacteria and regrowth over the course of the experiment or during storage were not verified, but since control bottles show limited

changes, microbial degradation was considered negligible at this timescale.

DOC concentrations were measured using a Shimadzu TOC-5000A carbon analyzer calibrated with potassium biphthalate. To characterize the chromophoric fraction of DOM (CDOM), absorbance scans were performed from 250 to 800 nm on a dual beam spectrophotometer (Cary 100, Varian) at a speed of 240 nm min^{-1} and slit width of 2 nm. Spectroscopic measurements were always run at natural pH and room temperature using 1 cm path length quartz cuvettes. Spectra were null-point adjusted and the absorption coefficient at 320 nm (a_{320}) was used to quantify CDOM. The spectral slope parameter S was calculated over two spectral bands (275–295 and 350–400 nm) according to Helms *et al* (2008), and the spectral slope curve S_λ was obtained according to Loiselle *et al* (2009) and using a wavelength interval size of 20 nm. The specific ultraviolet absorbance index SUVA (absorbance at 254 nm per unit DOC; Weishaar *et al* 2003) was also calculated.

Fluorescence properties of DOM were further characterized with excitation–emission matrices (EEMs) and the components extracted with PARAFAC (Stedmon *et al* 2003). EEM fluorescence was inner-filter corrected, blank-subtracted and Raman-normalised. A four-component model (C1–C4) was developed using a series of 36 aquatic systems located at the same site (including one creek, two large ponds, 21 runnel ponds and 12 polygonal ponds). PARAFAC modeling was performed according to Stedmon and Bro (2008) using the DOMFluor toolbox. Prior to modeling, Rayleigh scatter bands were excised (first order at each wavelength pair where excitation = emission \pm bandwidth; second order at each wavelength pair where emission = $2 \times$ excita-

tion \pm ($2 \times$ bandwidth)). The model was validated using split-half validation and random initialization.

The significance of light treatment as compared to control treatment in the dark was tested using repeated-measure analysis of variance on log-transformed data with the SAS software JMP 9.0.

3. Results

3.1. Pond limnological properties

Pond BYL1 is formed on top of a large depressed polygon with an irregular shape (possibly merging a few polygons; figure 1) and has a thick benthic microbial mat mainly composed of periphytic filamentous cyanobacteria (*Oscillatoriaceae*; Vézina and Vincent 1997). The maximum depth measured was 80 cm and the area was 354 m² (length of 32 m and width of 12 m). The chlorophyll *a* concentration (Chl *a*) in the water column was low (2.0 $\mu\text{g l}^{-1}$ on 19 July), as most production is benthic in this type of system (Rautio and Vincent 2006). Benthic Chl *a* was not measured in 2009, but varied from 1.1 to 34.8 $\mu\text{g cm}^{-2}$ in the study of Vézina and Vincent (1997) for 55 ponds sampled at this site. The pH was 8.66 and dissolved oxygen (DO) was supersaturated at the pond surface (12.1 mg O₂ l⁻¹ at 15h00 on 18 July). Total phosphorus (TP) reached 15.6 $\mu\text{g l}^{-1}$ at this period of the year, while soluble reactive phosphorus (SRP) was below the detection limit (0.2 $\mu\text{g l}^{-1}$).

Pond BYL38 is quite different from BYL1 as it sits on a melting ice wedge and presents clear signs of recent peat erosion (figure 1). It had a maximum pond depth of 80 cm, with a very irregular bottom. This pond is connected to a network of runnel ponds, thus the area of the specific segment sampled was estimated as about 55 m² from a high resolution image from WorldView-1. This less stable environment, caused by soil subsidence, precludes the establishment of microbial mats, and even though nutrients were more abundant (SRP and TP were 1.8 and 71.8 $\mu\text{g l}^{-1}$, respectively on 18 July) than in BYL1, planktonic Chl *a* concentration remained low (0.9 $\mu\text{g l}^{-1}$). The pH was 6.5 and DO was under-saturated at the surface (7.1 mg l⁻¹ at 10h00 on 19 July). A week later (25 July at 15h30), surface water pH and DO were even lower (6.1 and 3.9 mg l⁻¹, respectively), while they remained similar in BYL1.

3.2. Pond thermal structure

Thermistors (U12, Onset) installed at the surface of two ponds (~10 cm below interface) for a complete year indicated that the water froze around 24 September 2008 and the ice melted around 5 June 2009, so by extrapolation these dates correspond to approximately 111 days of open water. For thermistors placed in three ponds between July 2011 and July 2012, there were ~84–99 days of open water. In the summer, thermal stability of the water column will influence DOM photochemistry through an alternation of stratified periods, exposing top water layers to intense radiation, and mixing periods, renewing the water layers. Although ponds

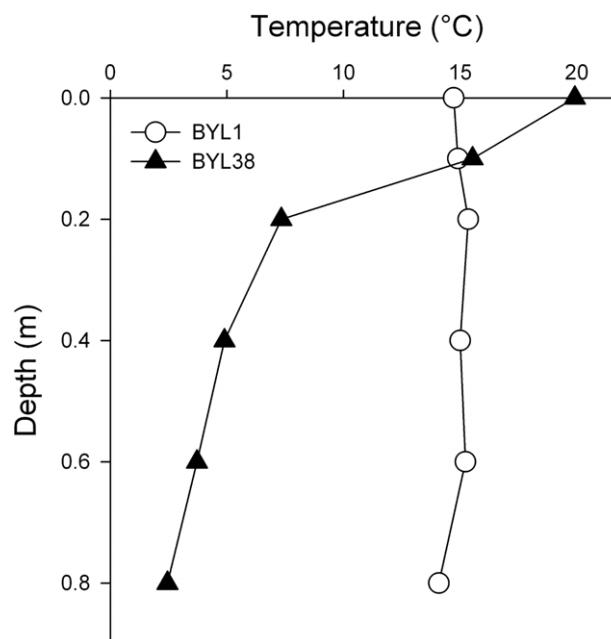


Figure 2. Example of late afternoon thermal profiles in ponds BYL1 and BYL38 during a sunny day in July.

are shallow and apparently exposed to moderate wind speed (average in July 2009 at 10 m above ground was 3 m s⁻¹), the sheltered topography of the long and narrow runnel ponds, often only ~1–3 m wide, their very small fetch, and efficient light absorption caused by high CDOM, often generate stratified conditions under the 24 h arctic sunlight. The thermal structure of the water column, followed at every 10–20 cm, showed mostly stratified conditions in BYL38 (figure 2), holding for the whole sampling period from 19 to 31 July 2009, a ubiquitous feature for this type of ponds. However, the temperature was mostly homogeneous in the polygonal pond BYL1, being more transparent (see below), and having less sheltered topography and a slightly longer fetch than BYL38. Mixed water column was also observed in another nearby polygonal pond.

3.3. Initial DOM characteristics of ponds

BYL38 had a higher DOC concentration than BYL1 (initial DOM properties given in table 1), but more importantly, its DOM or DOM–Fe complex was much more chromophoric, with absorptivity more than three times higher at 320 nm (or initial SUVA index of 5.0 m⁻¹ mg C⁻¹ l in BYL38 compared to 2.1 m⁻¹ mg C⁻¹ l in BYL1). Such high SUVA index for BYL38 is likely linked to the high total dissolved iron concentration measured in this pond (3.9 versus 0.3 mg l⁻¹ in BYL1). Thus, sunlight and particularly UV photons are attenuated more rapidly in BYL38. The absorption slope of BYL1 at 290 nm (*S*₂₉₀, calculated between 280 and 300 nm, table 1) was almost double the value in BYL38, and together with SR (*S*_{275–295}/*S*_{350–400} = 1.1 and 0.7 respectively in BYL1 and BYL38; Helms *et al* 2008), these indices indicate a lower DOM molecule size in the polygonal pond. However, Xiao *et al* (2013) also showed how high iron

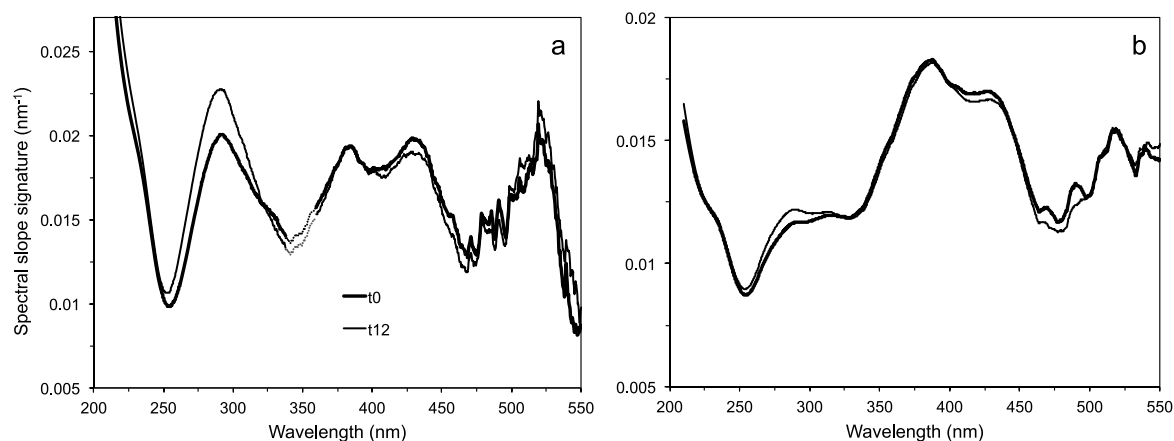


Figure 3. Spectral slope signature of DOM absorption (S_λ) from BYL1 (a) and BYL38 (b) at the beginning (t_0) and after 12 days (t_{12}) of incubation of filtered water under natural sunlight. Spectra shown are the average of four replicates. Dotted lines represent the extrapolated values after removing the band affected by lamp change by the spectrophotometer at 350 nm.

Table 1. Initial DOM properties (t_0) and changes (diff) after 12 days of incubation under natural sunlight (per cent differences given in parentheses), including dissolved organic carbon (DOC), absorption coefficient of CDOM at 320 nm (a_{320}), SUVA index (A_{254}/DOC), CDOM absorption slope at 290 nm (S_{290}), and four PARAFAC components extracted from EEMs of fluorescence (C1–C4, and the sum C1–C4, given in Raman units, RU). Significant treatment effect (ANOVA) is given in bold.

		DOC (mg l^{-1})	a_{320} (m^{-1})	SUVA ($\text{l m}^{-1} \text{ mg C}^{-1}$)	S_{290} (nm^{-1})	C1	C2	C3	C4	C1–C4
		(RU)								
BYL1	t_0	8.5	13.8	2.1	0.0195	0.63	0.84	0.25	0.52	2.2
	Diff	0.3 (3)	-3.4 (-25)	-0.34 (-16)	0.0029 (15)	-0.28 (-44)	-0.35 (-41)	-0.09 (-36)	-0.09^a (-18)	-0.8 (-36)
BYL38	t_0	13.1	73.5	5.0	0.0116	2.08	2.14	0.62	0.48	5.3
	Diff	-0.5 (-4)	-6.5 (-9)	-0.13 (-2.5)	0.0006 (5)	-0.76 (-37)	-0.41^a (-19)	-0.32 (-51)	-0.04 (-9)	-1.5 (-29)

^a All p -values < 0.001, except for C4 in BYL1 (0.0035) and C2 in BYL38 (0.0177).

concentrations, such as found in BYL38, can significantly lower DOM absorption slopes, thus interpretations of S_λ should be done cautiously when comparing waters of different Fe concentrations. The high DOC but rather low absorptivity of BYL1 also suggests that non-aromatic molecules such as some carbohydrates and protein-like compounds made up a larger fraction of DOM. The spectral slope signatures are shown in figure 3, where initial average values (t_0) are given by the thick lines. The BYL1 slope signature indeed shows a peak at the lower end of the spectrum (centered at 291 nm), which has been associated with algal-derived DOM in Loisellet *et al* (2009) for Chl *a*-rich natural waters or from algal cultures (peak centered at 280 nm). In BYL38, the signature is dominated by a wide peak in the blue region of the spectra (with maxima at 388 and 426 nm), associated with both humic and fulvic acids (peak at 390 nm); but in this case the trends are less clearly comparable with signatures found in the literature, possibly due to Fe content of this pond.

The fluorescence analyses showed that the EEMs of both ponds are distinct, with BYL1 having greater fluorescence in the amino acid region than BYL38 (figure 4). Our PARAFAC model identified four components (table 1), similar to components identified in previous studies (Stedmon and Markager 2005a, 2005b, Cory and McKnight 2005, table 2). In our study, C1–C3 are similar in peak fluorescence

to the humic-like fluorophores in Stedmon and Markager (2005a, 2005b), while our C4 is similar to the two protein-like fluorophores C4 and C6 in Stedmon and Markager (2005b), and tryptophan-like fluorescence found in other studies (table 2). C4 was found in larger proportion in BYL1 (23% at t_0 , compared to 9% in BYL38) than in BYL38. A greater proportion of protein-like fluorescence, presumably from microbial sources, supports the shape of S_λ and reflects the importance of smaller algal-derived CDOM molecules in this pond. Two of the humic-like components (C1, $\text{ex} = 340 \text{ nm/em} = 458 \text{ nm}$; C2, $\text{ex} = 300 \text{ nm/em} = 408 \text{ nm}$) were dominant in BYL38 (39 and 40% respectively for C1 and C2 at t_0), but were also abundant in BYL1 (28 and 37%). C3 had similar relative abundance in both ponds (11 and 12%), and its spectral characteristics ($\text{ex} = 270 \text{ and } 400 \text{ nm/em} = 516 \text{ nm}$) suggest that it is a terrestrial semiquinone-like compound similar to C5 in Cory and McKnight (2005) and to C7 in Stedmon and Markager (2005b).

3.4. DOM photolysis experiment

Over the course of this relatively short-term experiment, DOC did not change significantly in both ponds (table 1). However, several CDOM characteristics (a_{320} , S_{290} , C1–C4)

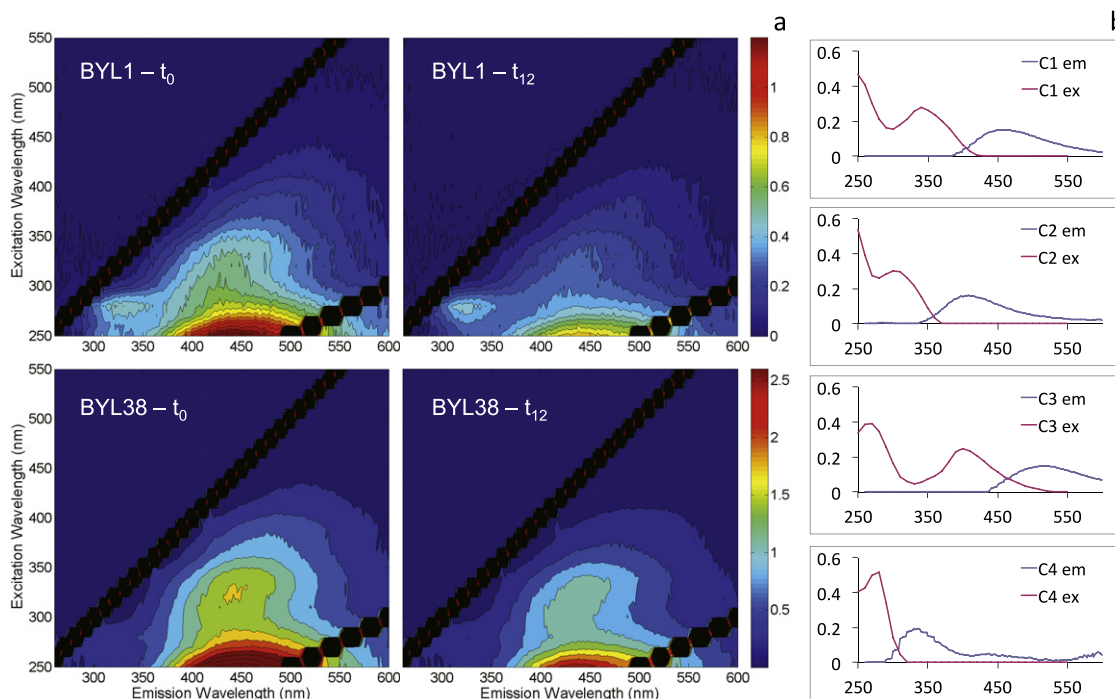


Figure 4. Excitation–emission matrices (EEMs) of fluorescence of the two experimental ponds at the beginning (t_0) and after 12 days (t_{12}) of filtered incubation water under natural sunlight (a), and emission spectra (blue line) and excitation spectra (red line) of the four extracted components from PARAFAC (b).

Table 2. Characteristics of the four components identified with the PARAFAC model in the present study, and of similar components previously identified in different aquatic systems (non-exhaustive list).

	C1	C2	C3	C4
Our study	250(340) ^a /458	250(300)/408	270(400)/516	280/330
Stedmon and Markager (2005a) Temperate estuary	C1 <250/448 terrestrial humic-like	C3 <250(305)/412 terrestrial humic-like	C2 <250(385)/504 terrestrial fulvic-like	C7 280/344 tryptophan-like
Stedmon and Markager (2005b) Norwegian fjord	C1 240(355)/476 humic-like	C2 240(340)/398 humic-like C3 295/398 humic-like	C7 (275)420/488 humic-like	C4 275/306(338) protein-like C6 280/338 tryptophan-like
Cory and McKnight (2005) Polar lakes and other freshwaters	C1 (275)340/450	C12 250(300)/388 quinone-like	C5 290(380)/520 semiquinone-like	C13 280/<350 tryptophan-like
Yamashita <i>et al</i> (2008) Marine coastal waters	C1 <260/458 terrestrial humic-like C2 345/433 terrestrial humic-like	—	C3 (275)390/479 terrestrial humic-like	—
Mladenov <i>et al</i> (2011) Alpine lakes	—	C2 240(290)/406 humic-like	—	C3 240(300)/338 amino acid-like
Tank <i>et al</i> (2011) Arctic lakes	—	C1 250(310)/422 humic-like	C2 265(365)/487 fulvic-like	C3 280/340 protein-like

^a Wavelengths in parentheses indicate the less intense secondary peak of fluorescence emission.

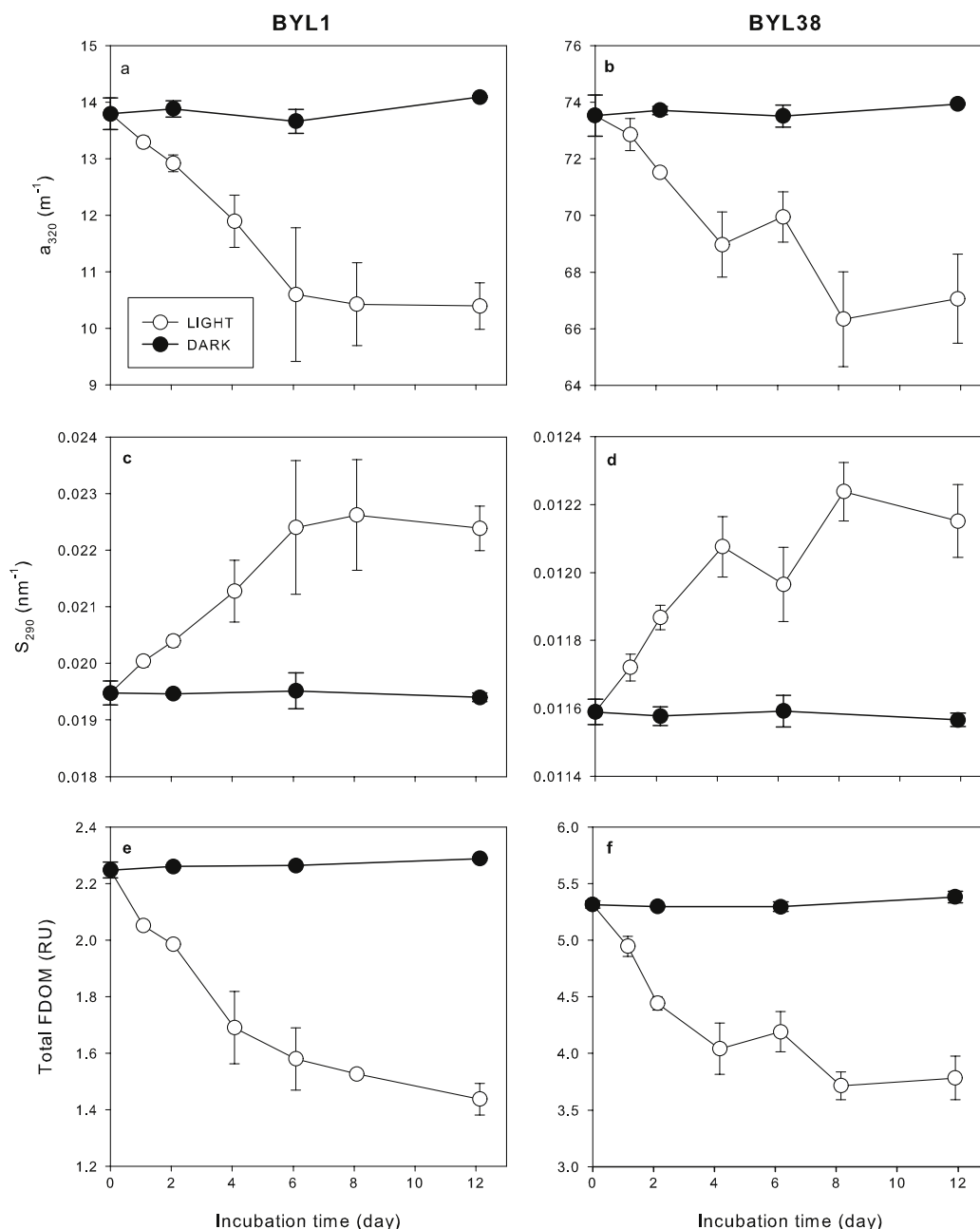


Figure 5. DOM properties over 12 days of incubation under natural sunlight of filtered water from ponds BYL1 ((a), (c), (e)) and BYL38 ((b), (d), (f)), including the absorption coefficient at 320 nm (a_{320}), the slope of absorption at 290 nm (S_{290}) and the total fluorescence from four PARAFAC components (FDOM).

changed significantly ($p < 0.02$, except for C4 in BYL38 where $p = 0.3468$; table 1, figure 5). The relative CDOM loss, measured as percentage loss of a_{320} over 12 days, was approximately three times larger in BYL1 than in BYL38, but the absolute loss (in m^{-1}) was 2 times larger in BYL38 (figures 5(a) and (b)). Increase in slope S_{290} (figures 5(c) and (d); an index similar to $S_{270-295}$ in Helms *et al* (2008)), at the wavelength where the largest changes were observed over the whole spectrum (figure 3), suggests a decrease in size of CDOM molecules over time. Both relative and absolute changes in S_{290} were larger in BYL1. A second slope index fixed at 375 nm (S_{375} , i.e. integrated from 365 to 385 nm,

similar to $S_{350-400}$ developed by Helms *et al* 2008), only showed significant decrease in BYL38 ($p = 0.0012$). Another region of the spectra where a significant slope decrease was found in both ponds at the end of the experiment is around 425 nm (S_{425} calculated between 415 and 435 nm; figure 3). In terms of CDOM fluorescence (EEMs), all four components decreased over 12 days (the sum C1–C4 is presented as total FDOM in figures 5(e) and (f)), but the relative proportion of each component also changed, i.e. the components were not lost at the same rate (table 1, but see below).

The loss rate of CDOM (a_{320} , total FDOM; figure 5) declined after ~6 days, but the properties did not follow

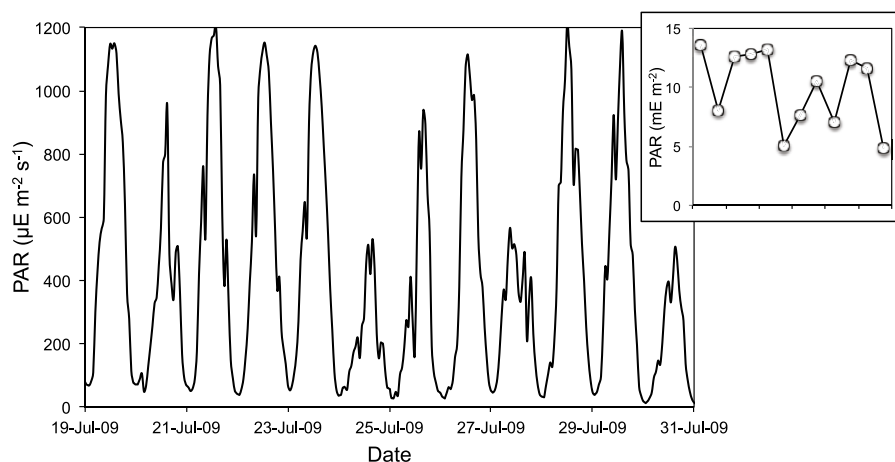


Figure 6. Photosynthetically available radiation (PAR) measured at the CEN SILA station (www.cen.ulaval.ca) every hour (average over preceding hour) along the 12 days of incubation (19–30 July 2009), and cumulative PAR dose over the preceding 24 h each day at 22 h when sampling was done (inset).

Table 3. Linear loss rates (% loss rates in parentheses) of DOM (a_{320} and four EEMs components) over the first four days of incubation as a function of time (bold means regression p -values < 0.019).

Pond	a_{320} ($\text{m}^{-1} \text{d}^{-1}$)	C1	C2	C3	C4	C1–C4
		(RU d^{-1})				
BYL1	0.469 (3.4)	0.045 (7.2)	0.062 (7.3)	0.015 (5.7)	0.015 (2.9)	0.137 (6.1)
BYL38	1.142 (1.6)	0.206 (9.9)	0.143 (6.7)	0.072 (11.7)	0.017 (3.6)	0.439 (8.3)

a first-order logarithmic decay (i.e., log decay also slowed down). Therefore, linear loss rates over the first four days were calculated as a function of time (table 3). Initial loss rates of color at 320 nm were calculated as 3.4 and 1.6% per day in BYL1 and BYL38, respectively. The initial loss rate of C4 (tryptophan-like) was the lowest of all four components for both ponds (respectively 2.9 and 3.6% per day), while the highest loss rate was observed for C3 in BYL38 (11.7% per day), and the other rates varied between 5.7 and 9.9% per day. These rates were also calculated as a function of the cumulative irradiance dose received at depth of incubation as computed from Hydrolight (see below), but the trends were not different (i.e., larger absolute loss rates of color and fluorescence in BYL38, and only larger relative loss rates of a_{320} in BYL1). For example, the loss rate of color at 320 nm over 4 days was 0.0105 and 0.0311 $\text{m}^{-1} (\text{E m}^{-2})^{-1}$, respectively for BYL1 and BYL38 (not shown).

Although radiation in the UV range, the most relevant wavelengths for DOM photolysis (Vähätalo *et al* 2000), was not measured at this site, a decreasing trend over the incubation period was expected as a result of the slightly more cloudy conditions in the second half of the experiments shown by incident photosynthetically available radiation (PAR; figure 6, inset presents PAR summed over the preceding 24 h at 22h00 each evening, the approximate sampling time). In order to estimate the radiation dose received at the sampling depth, we used the Hydrolight radiative transfer model (Sequoia Scientific Inc., USA) to

compute incident spectra at this latitude and date, and, for simplification, we assumed the exposure of water samples was that of an optically thin solution, and attenuation was mainly generated by DOM absorption (i.e., $K_d = a_{\text{CDOM}}$). The spectra generated at 5 cm depth for a clear day when the sun is at the zenith (13h00) and associated values of integrated UVB (wavelengths from 300–320 nm), UVA (320–400 nm) and PAR, in W m^{-2} of these modeled spectra (figure 7) indicate that there were respectively 22, 4 and 1.2 times more UVB, UVA and PAR at the incubation depth in BYL1 compared to BYL38. The difference is most likely even larger due to the more abundant suspended solids in BYL38 (8.0 mg l^{-1} compared to 1.3 mg l^{-1} in BYL1 in 2010), which probably contribute substantially to scattering and thus to the attenuation of sunlight. These spectra were also used to compute the potential photomineralization of DOC into DIC (see section 4.3).

4. Discussion

Thaw ponds are abundant in the arctic landscape, and in certain regions they are becoming more widespread as permafrost thaws (Payette *et al* 2004, Jorgenson *et al* 2006, Takakai *et al* 2008). They are hotspots for microbial activity and GHG production when they are rich in organic C and nutrients (Laurion *et al* 2010). Under certain geomorphological conditions, such as those found on Bylot Island, ponds are very small and shallow; thus they are

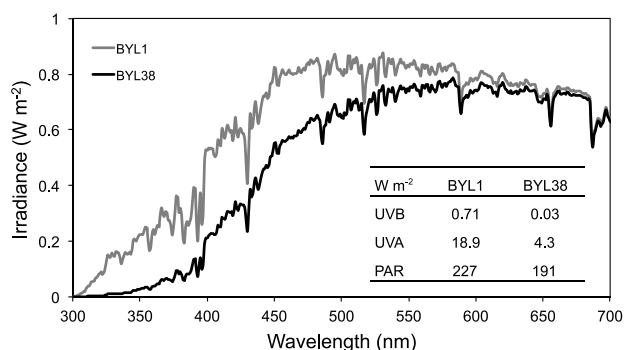


Figure 7. Spectral irradiance at depth of incubation (5 cm) as simulated using the Hydrolight model for a sunny day at 13 h on 24 July, at 73°09'N, 79°59'W, and considering K_d equals DOM absorption, and integrated energy for UVB, UVA and PAR (inset).

exposed to large photon flux in the summer. In the two ponds studied here, CDOM loss rate was relatively rapid at the surface (table 3), indicating a dynamic transformation of this organic pool. However, the photolysis rates calculated at 440 nm (photolysis rate coefficient k_b of 7 and 2×10^{-4} ($E\ m^{-2}$)⁻¹ respectively for BYL1 and BYL38, using a negative exponential fit on the first 4–8 days in order to compare with the results of Reche *et al* 1998) were at the low end compared to the range of values obtained in a series of 30 temperate lakes for similar cumulative sunlight doses, reaching $\sim 500\ E\ m^{-2}$ at the end of incubation period ($7\text{--}46 \times 10^{-4}$ ($E\ m^{-2}$)⁻¹).

Roehm *et al* (2009) have shown that soil extracts from permafrost peat in northern Sweden were rapidly consumed by bacteria in the dark ($0.4\ mg\ C\ l^{-1}\ d^{-1}$). Laboratory incubations and field experiments with thawed Yedoma organic matter from Siberia and Alaska also showed a relatively quick decomposition upon thawing, resulting in respiration rates of initially $10\text{--}40\ mg\ C\ l^{-1}\ d^{-1}$ and then $0.5\text{--}5\ mg\ C\ l^{-1}\ d^{-1}$ over several years (Zimov *et al* 2006). The action of light is most likely accelerating these carbon consumption rates and therefore should be taken into account in C cycling.

4.1. Sources of DOM in thaw ponds

Compared to polygonal ponds, runnel ponds have larger DOC concentrations, and especially more terrestrially derived chromophoric DOM (higher a_{320} and SUVA), although part of this color is possibly coming from the complex DOM–Fe, and more humic molecules (smaller S_λ , larger % of humic-like C1, smaller % of protein-like C4). Such higher humic contents in runnel ponds were confirmed in other ponds from the same site, with an average of $28 \pm 2\%$ of C1 and $21 \pm 5\%$ of C4 for 10 polygonal ponds compared to $37 \pm 2\%$ of C1 and $10 \pm 2\%$ of C4 for 14 runnel ponds (data not shown), and supports a great contribution of eroding peat as a source of large humic-like organic molecules to pond water. The larger contribution of DOM from a terrestrial origin in runnel ponds is further evidenced by its DOC- $\delta^{13}C$ signature that was $-27.4 \pm 0.5\%$ ($n = 6$) compared to $-24.6 \pm 1.0\%$ in

polygonal ponds ($n = 11$; July 2007; unpublished results). Tank *et al* (2011) also found such evidence of a large contribution of permafrost soil erosion to the DOM pool of small lakes with thermokarst influence in the Mackenzie Delta.

By contrast, the larger proportion of C4 (tryptophan-like) in BYL1, representing 23% of total fluorescence compared to 9% in BYL38, suggests that thick and active cyanobacterial mats, characteristic of polygonal ponds, significantly contributed to the DOM pool.

4.2. Photobleaching rates

Humic type DOM molecules are generally considered highly photoreactive (Obernosterer and Benner 2004). In fact, the largest change in the absorption spectral slope index S_λ occurred below $\sim 310\ nm$ in the studied thaw ponds (figure 3), which is consistent with spectral slope calculations for photolysis of humic DOM in Argentinian lakes (Galgani *et al* 2011). Therefore, we expect the more humic OM mobilized by thawing of permafrost peaty soils to be highly susceptible to photolysis.

Indeed, even though there was 4.4 times less UVA in BYL38 (at 5 cm) than in BYL1 (figure 7), photobleaching of DOM molecules was faster in BYL38 (table 3). Photobleaching efficiency is known to be optimal in the UVA waveband, where quantum yield \times photon flux density is maximal (Vähätalo *et al* 2000). Despite that, when calculated per unit of total energy or per unit energy at 360 or 320 nm (not shown) at the depth of incubation, CDOM loss rates were still faster in BYL38. Gareis (2007) also found increased photolysis rate when CDOM was higher in a series of shallow arctic lakes of the MacKenzie Delta. As a first-order decay process, photolysis is a function of concentration, and the greater % loss of absorbance and fluorescence in BYL38 is likely related to the higher concentration of CDOM and FDOM in this runnel pond. In addition, the more humic quality of DOM in BYL38 compared to BYL1 may also contribute to the greater loss of CDOM and FDOM. Photodegradation has been shown to preferentially degrade microbial humic-like components (C1, C2, C3 and C7 in Stedmon and Markager (2005b)) and terrestrial humic-like components (C1 and C2 in Stedmon and Markager (2005a); C1 and C2 in Yamashita *et al* (2008)), whereas exposure to UV or visible light had less of an effect on protein-like fluorophores (C4 and C6 in Stedmon and Markager (2005b)). Our results confirm these earlier findings; the protein-like component C4 was the most photo-resistant of the four components, and the humic-like components identified were the most photo-labile in both ponds.

Higher pH was shown to increase the absorption cross-section of chromophores (Pace *et al* 2012), but the larger pH of BYL1 seemed not sufficient to generate a higher photolysis rate for this pond. In BYL38, it is also possible that the photo-reduction of DOM-complexed Fe(III) into Fe(II) would reduce the measured UV absorbance, and explain part of the larger photobleaching rate observed. However, decrease in the SUVA over 12 days is not significant in BYL38

(table 1), which is at the lower end of the UV spectrum where photo-reduction should be most efficient. This suggests that photo-reduction of DOM-complexed Fe(III) was not important, potentially because of the limited exposure to shorter UV wavelengths ($\sim 2\%$ of incident UVB and 16% of incident UVA remains at 5 cm) and the relatively high pH (Waite and Morel 1984).

Using initial decay rates, it would take 29 days to completely bleach CDOM at the surface of BYL1, or 63 days at the surface of BYL38 due to its more concentrated and colored DOM. In Canadian thaw ponds, which have open water for ~ 85 – 110 days each summer, photolysis can thus represent a major C cycling mechanism. This is especially important for ponds with small catchments, lying in flat polygonal landscapes and influenced by evaporation (using $\delta^{18}\text{O}$, Negandhi 2013). Evaporation could accelerate bleaching by reducing pond depth, thereby exposing a greater proportion of the pond's CDOM to sunlight. Interestingly, on a relative scale, the loss rate of color was slower than the loss rate of fluorescence, and fluorescence loss was faster in BYL38 than in BYL1 (12 compared to 16 days to completely bleach FDOM, respectively).

The above calculations were done considering that all CDOM is similarly photoreactive. The decay of absorbance and fluorescence, which plateaus after four days (figure 5), suggests this is not the case. Microbial regrowth in incubation bottles was likely limited as seen from the flat shape of the control curves, unless regrowth was only stimulated under sunlight, so recycling of DOM would not explain this deceleration. Moreover, if pond mixing regimes were included, we might expect greater renewal of DOM molecules in the well-mixed BYL 1 and more efficient photolysis than what was observed over the 12 day assays. By contrast, photolysis might be limited by the thermal structure of BYL38 (figure 2) and surface incubation may better represent local conditions.

4.3. Phototransformation versus photomineralization

Over an incubation period of 12 days, significant DOC loss could not be detected. The relatively small DOC loss concurrent with significant CDOM loss indicates that photolysis resulted mainly in a change in molecular properties (photobleaching) rather than in DOC mineralization. The idea that large CDOM molecules are broken into smaller ones when exposed to sunlight, as suggested in other studies based on changes in S_λ (Galgani *et al* 2011) and mass spectrometry or molecular filtration (Waiser and Roberts 2004), is also supported by our fluorescence results. Although all fluorescent components decreased over time under 'microbial free' conditions ($0.2 \mu\text{m}$ -filtered) they did so at different rates. More highly conjugated CDOM molecules can undergo both direct and indirect photochemical reactions via hydroxyl and other radicals, which preferentially degrade aromatic functional groups and may result in the presence of smaller *non-fluorescing* molecules. This would explain the absence of DOC loss concurrent with large CDOM losses. The influence of DOM–Fe complexes on changes in

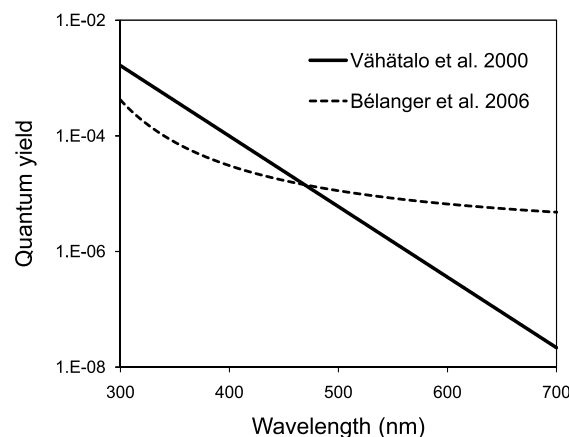


Figure 8. Quantum yield of photochemical mineralization (DOC into DIC) from 300 to 700 nm, computed by Bélanger *et al* (2006) for the coastal arctic ocean, and by Vähätalo *et al* (2000) for a humic lake.

the optical properties of DOM should again be considered, as Fe(III) is known to be more effective at quenching the fluorescence of DOM (Ohno *et al* 2008) than Fe(II) (Poulin and Aiken 2010). Therefore, interpretations based only on optical properties of DOM are somehow limited, and mass spectrometry, together with Fe speciation data, would help to further understand the implications of photolysis on the transformation of such complex assemblages of DOM molecules (Seitzinger *et al* 2005, Sleighter and Hatcher 2007).

The rate of photochemical mineralization of DOC at a specific depth depends on three wavelength-dependent parameters: the amount of light received at this depth, the absorption by CDOM and the quantum yield (Φ_λ), defined as the moles of DIC produced per mole of absorbed photons. The Φ_λ has been calculated for two contrasting aquatic environments, the coastal Arctic Ocean (Bélanger *et al* 2006) and a Finnish humic lake (Vähätalo *et al* 2000). These two models, having fairly different shapes (figure 8), were applied to the present data set in order to estimate the potential DOC loss for the two ponds at the incubation depth, and to determine if 12 days were sufficient to generate visible changes in DOC. A few assumptions were made to simplify the calculations: weather conditions were considered sunny during the 12 days of incubation, incident light was computed from Hydrolight, light attenuation was approximated to a_{CDOM} as measured along the incubation, and the depth of incubation was fixed at 5 cm for an optically thin solution. The Vähätalo model predicted DOC loss of 0.9 and 5.9 mg l^{-1} after 12 days, respectively for BYL1 and BYL38, while the Bélanger model predicted 0.2 and 1.4 mg l^{-1} . Measured values of $0.3 \text{ mg DOC l}^{-1}$ gained in BYL1 and 0.5 mg l^{-1} lost in BYL38, which are insignificant changes, were lower than both model predictions but closer to the Bélanger results. The lower measured values may be due in part to some cloud cover occurring in the second half of the incubation period, lowering incident PAR to 78% of what would be received under 12 sunny days (see figure 6). It could also result from increased light attenuation caused by the presence of suspended particles, especially in BYL38 where total

suspended solids reached 9.1 mg l^{-1} (2008 unpublished data; about five times larger than in BYL1). Nevertheless, this exercise suggests that the Bélanger model better represents the susceptibility of Bylot pond DOM to photochemical mineralization. It also indicates that quantum yield spectra specific for each type of ecosystems or DOM assemblages are needed to better estimate DOC losses through modeling under changing environmental conditions.

5. Conclusions

Photochemical transformation of DOM has been described as an important mechanism to generate more labile compounds from large humic DOM molecules, as evidenced by increased bacterial production and bacterial growth efficiency after exposure to sunlight. The present study suggests that CDOM in both polygon and runnel thaw ponds may contain a large fraction of humic molecules derived from terrestrial sources, with >66% of fluorescence derived from humic-like molecules. The action of light resulted in significant and quick CDOM loss in our study, which has the potential to improve the bioavailability of the organic matter mobilized by permafrost thawing and accelerate its mineralization, especially in the abundant shallow aquatic systems of the high Arctic. The length of the ice-free season, the lake mixing regime, and the movement of water and organic matter between terrestrial and aquatic systems are all likely to be affected by climate change; thus they will also influence photolysis rates and have important consequences for microbial mineralization. Photolysis should therefore be taken into account in global estimations of future GHG emissions from inland waters. Future work will need to assess DOM microbial degradation rates under natural light conditions, including direct measurements of CO_2 production rates, bacterial production and respiration, and methods accounting for the non-chromophoric fraction of DOM.

Acknowledgments

We thank P-G Rossi and V Gélinas for their efficient help in the field and laboratory, D Sarrazin for collecting meteorological data, S Watanabe for computing incident spectra with Hydrolight, M Ricci for his code and help with the spectral slope calculation, S Loiselle and A V Vähätalo for fruitful discussions, G Gauthier, the Centre for Northern Studies, the Polar Continental Shelf Project and Parks Canada for logistical support, and ArcticNet NCE, NSERC and IPY for the financial support.

References

Abnizova A, Siemens J, Langer M and Boike J 2012 Small ponds with major impact: the relevance of ponds and lakes in permafrost landscapes to carbon dioxide emissions *Glob. Biogeochem. Cycles* **26** GB2041

Anesio A M, Granéli W, Aiken G R, Kieber D J and Mopper K 2005 Effect of humic substance photodegradation on bacterial growth and respiration in lake water *Appl. Environ. Microbiol.* **71** 6267–75

Bélanger S, Xie H, Krotkov N, Larouche P, Vincent W F and Babin M 2006 Photomineralization of terrigenous dissolved organic matter in Arctic coastal waters from 1979 to 2003: interannual variability and implications of climate change *Glob. Biogeochem. Cycles* **20** GB4005

Bertilsson S and Allard B 1996 Sequential photochemical and microbial degradation of refractory dissolved organic matter in a humic freshwater system *Arch. Hydrobiol. Adv. Limnol.* **48** 133–41

Bertilsson S and Jones J B 2003 Supply of dissolved organic matter to aquatic ecosystems: autochthonous sources *Aquatic Ecosystems: Interactivity of Dissolved Organic Matter* ed S E G Findlay and R L Sinsabaugh (New York: Academic)

Bertilsson S and Tranvik L J 2000 Photochemical transformation of dissolved organic matter in lakes *Limnol. Oceanogr.* **45** 753–62

Bretton J, Vallières C and Laurion I 2009 Limnological properties of permafrost thaw ponds in northeastern Canada *Can. J. Fish. Aquat. Sci.* **66** 1635–48

Chen W, Westerhoff P, Leenheer J A and Booksh K 2003 Fluorescence excitation–emission matrix regional integration to quantify spectra for dissolved organic matter *Environ. Sci. Technol.* **37** 5701–10

Cory R M and McKnight D M 2005 Fluorescence spectroscopy reveals ubiquitous presence of oxidized and reduced quinones in dissolved organic matter *Environ. Sci. Technol.* **39** 8142–9

Fortier D 2013 personal communication

Fortier D and Allard M 2004 Late Holocene syngenetic icewedge polygons development, Bylot Island, Canadian Arctic archipelago *Can. J. Earth Sci.* **41** 997–1012

Galgani L, Tognazzi A, Rossi C, Ricci M, Galvez J A, Dattilo A M, Cozar A, Bracchini L and Loiselle S A 2011 Assessing the optical changes in dissolved organic matter in humic lakes by spectral slope distributions *J. Photochem. Photobiol. B* **102** 132–9

Gareis J A L 2007 Underwater irradiance attenuation and photobleaching of chromophoric dissolved organic matter in shallow arctic lakes of the Mackenzie Delta NWT *MSc Thesis* Simon Fraser University

Gareis J A L, Lesack L F W and Bothwell M L 2010 Attenuation of *in situ* UV radiation in Mackenzie Delta lakes with varying dissolved organic matter compositions *Water Resour. Res.* **46** W09516

Granéli W, Lindell M and Tranvik L J 1996 Photo-oxidative production of dissolved inorganic carbon in lakes of different humic content *Limnol. Oceanogr.* **41** 698–706

Grosse G, Romanovsky V E, Jorgenson T, Walter Anthony K, Brown J and Overduin P P 2011 Vulnerability and feedbacks of permafrost to climate change *EOS Trans. AGU* **92** 73–4

Helms J R, Stubbins A, Ritchie J D, Minor E C, Kieber D J and Mopper K 2008 Absorption spectral slopes and slope ratios as indicators of molecular weight, source, and photobleaching of chromophoric dissolved organic matter *Limnol. Oceanogr.* **53** 955–69

IPCC (International Panel on Climate Change) 2007 Summary for policymakers *Climate Change 2007: The Physical Science Basis. Contribution of Working Group I to the Fourth Assessment Report of the Intergovernmental Panel on Climate Change* (Cambridge: Cambridge University Press)

Johannessen S C and Miller W L 2001 Quantum yield for the photochemical production of dissolved inorganic carbon in seawater *Mar. Chem.* **76** 271–83

Jorgenson M T, Shur Y L and Pullman E R 2006 Abrupt increase in permafrost degradation in Arctic Alaska *Geophys. Res. Lett.* **33** L02503

Kuhry P, Ping C-L, Tarnocai C, Schuur E A G and Zimov S 2009 Report from the international permafrost association: carbon pools in permafrost regions *Permafrost Periglac. Process.* **20** 229–34

Laurion I, Vincent W F, Retamal L, Dupont C, Francus P and Pienitz R 2010 Variability in greenhouse gas emissions from permafrost thaw ponds *Limnol. Oceanogr.* **55** 115–33

- Lehner B and Döll P 2004 Development and validation of a global database of lakes, reservoirs and wetlands *J. Hydrol.* **296** 1–22
- Lindell M J, Granéli W and Tranvik L J 1995 Enhanced bacterial growth in response to photochemical transformation of dissolved organic matter *Limnol. Oceanogr.* **40** 195–9
- Loiselle S A, Bracchini L, Dattilo A M, Ricci M, Tognazzi A and Rossi C 2009 Optical characterization of chromophoric dissolved organic matter using wavelength distribution of absorption spectral slopes *Limnol. Oceanogr.* **54** 590–7
- Mladenov N *et al* 2011 Dust inputs and bacteria influence dissolved organic matter in clear alpine lakes *Nature Commun.* **2** 405
- Muster S, Langer M, Heim B, Westermann S and Boike J 2012 Subpixel heterogeneity of ice-wedge polygonal tundra: a multiscale analysis of land cover and evapotranspiration in the Lena River Delta, Siberia *Tellus B* **64** 17301
- Negandhi K 2013 personal communication
- Obernosterer I and Benner R 2004 Competition between biological and photochemical processes in the mineralization of dissolved organic carbon *Limnol. Oceanogr.* **49** 117–24
- Ohno T, Amirbahman A and Bro R 2008 Parallel factor analysis of excitation–emission matrix fluorescence spectra of water soluble soil organic matter as basis for the determination of conditional metal binding parameters *Environ. Sci. Technol.* **42** 186–92
- Pace M L, Reche I, Cole J J, Fernández-Barbero A, Mazuecos I P and Prairie Y T 2012 pH change induces shifts in the size and light absorption of dissolved organic matter *Biogeochemistry* **108** 109–18
- Payette S, Delwaide A, Caccianiga M and Beauchemin M 2004 Accelerated thawing of subarctic peatland permafrost over the last 50 years *Geophys. Res. Lett.* **31** L18208
- Poulin B and Aiken G R 2010 The effects of ferric and ferrous iron on the optical properties of dissolved organic matter *2010 Fall Mtg of the American Geophysical Union Abstract #B111-03*
- Prowse T, Alfredsen K, Beltaos S, Bonsal B, Duguay C, Korhola A, McNamara J, Vincent W F, Vuglinsky V and Weyhenmeyer G A 2011 Effects of changes in arctic lake and river ice *Ambio* **40** 63–74
- Rautio M, Dufresne F, Laurion I, Bonilla S, Vincent W F and Christoffersen K S 2011 Shallow freshwater ecosystems of the circumpolar Arctic *Ecoscience* **18** 204–22
- Rautio M and Vincent W F 2006 Benthic and pelagic food resources for zooplankton in shallow high-latitude lakes and ponds *Freshwater Biol.* **51** 1038–52
- Reche I, Pace M L and Cole J J 1998 Interactions of photobleaching and inorganic nutrients in determining bacterial growth on colored dissolved organic carbon *Microb. Ecol.* **36** 270–80
- Reche I, Pace M L and Cole J J 1999 Relationship of trophic and chemical conditions to photobleaching of dissolved organic matter in lake ecosystems *Biogeochemistry* **44** 259–80
- Roehm C L, Giesler R and Karlsson J 2009 Bioavailability of terrestrial organic carbon to lake bacteria: the case of a degrading subarctic permafrost mire complex *J. Geophys. Res.* **114** G03006
- Rowland J C *et al* 2010 Arctic Landscapes in Transition: Responses to Thawing Permafrost *EOS Trans. AGU* **91** 229–36
- Seitzinger S P, Hartnett H, Lauck R, Mazurek M, Minegishi T, Spyres G and Styles R 2005 Molecular-level chemical characterization and bioavailability of dissolved organic matter in stream water using electrospray-ionization mass spectrometry *Limnol. Oceanogr.* **50** 1–12
- Sleighter R L and Hatcher P G 2007 Molecular-level chemical characterization and bioavailability of dissolved organic matter in stream water using electrospray-ionization mass spectrometry *J. Mass Spectrom.* **42** 559–74
- Smith L C, Sheng Y and MacDonald G M 2007 A first pan-arctic assessment of the influence of glaciation, permafrost, topography and peatlands on Northern Hemisphere lake distribution *Permafrost Periglac. Process.* **18** 201–8
- Stedmon C A and Bro R 2008 Characterizing dissolved organic matter fluorescence with parallel factor analysis: a tutorial *Limnol. Oceanogr.: Methods* **6** 572–9
- Stedmon C A and Markager S 2005a Resolving the variability in dissolved organic matter fluorescence in a temperate estuary and its catchment using PARAFAC analysis *Limnol. Oceanogr.* **50** 686–97
- Stedmon C A and Markager S 2005b Tracing the production and degradation of autochthonous fractions of dissolved organic matter by fluorescence analysis *Limnol. Oceanogr.* **50** 1415–26
- Stedmon C A, Markager S and Bro R 2003 Tracing dissolved organic matter in aquatic environments using a new approach to fluorescence spectroscopy *Mar. Chem.* **82** 239–54
- Takakai F, Desyatkin A R, Lopez C M L, Fedorov A N, Desyatkin R V and Hatano R 2008 CH₄ and N₂O emissions from a forest-alas ecosystem in the permafrost taiga forest region, eastern Siberia, Russia *J. Geophys. Res. Biogeosci.* **113** G02002
- Tank S E, Lesack L F W, Gareis J A L, Osburn C L and Hesslein R H 2011 Multiple tracers demonstrate distinct sources of dissolved organic matter to lakes of the Mackenzie Delta, western Canadian Arctic *Limnol. Oceanogr.* **56** 1297–309
- Tank S E, Lesack L F W and Hesslein R H 2009 Northern delta lakes as summertime CO₂ absorbers within the arctic landscape *Ecosystems* **12** 144–57
- Tranvik L J *et al* 2009 Lakes and reservoirs as regulators of carbon cycling and climate *Limnol. Oceanogr.* **54** 2298–314
- Vähätalo A V, Salkinoja-Salonen M, Taalas P and Salonen K 2000 Spectrum of the quantum yield for photochemical mineralization of dissolved organic carbon in a humic lake *Limnol. Oceanogr.* **45** 664–76
- Vähätalo A V and Wetzel R G 2004 Photochemical and microbial decomposition of chromophoric dissolved organic matter during long (months–years) exposures *Mar. Chem.* **89** 313–26
- Vézina S and Vincent W F 1997 Arctic cyanobacteria and limnological properties of their environment: Bylot Island, Northwest Territories, Canada (73°N, 80°W) *Polar Biol.* **17** 523–34
- Vincent W F, Laurion I, Pienitz R and Walter Anthony K M 2013 Climate impacts on arctic lake ecosystems *Climatic Change and Global Warming of Inland Waters: Impacts and Mitigation for Ecosystems and Societies* ed C R Goldman, M Kumagai and R D Robarts (New York: Wiley)
- Waiser M J and Robarts R D 2004 Photodegradation of DOC in a shallow prairie wetland: evidence from seasonal changes in DOC optical properties and chemical characteristics *Biogeochemistry* **69** 263–84
- Waite T D and Morel F M M 1984 Photoreductive dissolution of colloidal iron oxides in natural waters *Environ. Sci. Technol.* **18** 860–8
- Walter K M, Smith L C and Chapin F S III 2007 Methane bubbling from northern lakes: present and future contribution to the global CH₄ budget *Phil. Trans. R. Soc. A* **365** 1657–76
- Weishaar J L, Aiken G R, Depaz E, Bergamaschi B, Fram M and Fujii R 2003 Evaluation of specific ultra-violet absorbance as an indicator of the chemical composition and reactivity of dissolved organic carbon *Environ. Sci. Technol.* **37** 4702–8
- Xiao Y-H, Sara-Aho T, Hartikainen H and Vähätalo A V 2013 Contribution of ferric iron to light absorption by chromophoric dissolved organic matter *Limnol. Oceanogr.* **58** 653–62
- Yamashita Y, Jaffé R, Maie N and Tanoue E 2008 Assessing the dynamics of dissolved organic matter (DOM) in coastal environments by excitation emission matrix fluorescence and parallel factor analysis (EEM–PARAFAC) *Limnol. Oceanogr.* **53** 1900–8
- Zepp R G, Erickson D J III, Paul N D and Sulzberger B 2007 Interactive effects of solar UV radiation and climate change on biogeochemical cycling *Photochem. Photobiol. Sci.* **6** 286–300
- Zimov S A, Schuur E A G and Chapin F S III 2006 Permafrost and the global carbon budget *Science* **312** 1612–3